Research Article

Zeeshan Khan, Haroon Ur Rasheed, Tawfeeq Abdullah Alkanhal, Murad Ullah, Ilyas Khan*, and Iskander Tlili

Effect of magnetic field and heat source on Upper-convected-maxwell fluid in a porous channel

https://doi.org/10.1515/phys-2018-0113
Received Apr 12, 2018; accepted Jun 05, 2018

Abstract: The effect of magnetic field on the flow of the UCMF (Upper-Convected-Maxwell Fluid) with the property of a heat source/sink immersed in a porous medium is explored. A shrinking phenomenon along with the permeability of the wall are considered. The governing equations for the motion and transfer of heat of the UCMF along with boundary conditions are converted into a set of coupled nonlinear mathematical equations. Appropriate similarity transformations are used to convert the set of nonlinear partial differential equations into nonlinear ordinary differential equations. The modeled ordinary differential equations have been solved by the Homotopy Analysis Method (HAM). The convergence of the series solution is established. For the sake of comparison, numerical (ND-Solve method) solutions are also obtained. Special attention is given to how the non-dimensional physical parameters of interest affect the flow of the UCMF. It is observed that with the increasing Deborah number the velocity decreases and the temperature inside the fluid increases. The results show that the velocity and temperature distribution increases with a porous medium. It is also observed that the magnetic parameter has a decelerating effect on velocity while the temperature profiles increases in the entire domain. Due to the increase in Prandtl number the temperature profile increases. It is also observed that the heat source enhance the thermal conductivity and increases the fluid temperature while the heat sink provides a decrease in the fluid temperature.

Keywords: Heat source/sink, UCMF, Magnetohydrodynamic, Porisity, Shrinking channel

PACS: 45.10.-b, 47.10.-g, 47.55.pb, 47.56.+r

Nomenclature

β	Deborah number
η	Similarity variable
ν	Kinematic viscosity (m^2s^{-1})
θ	Dimensionless temperature
φ	Stream function
λ_1	Internal heat generation/absorption parameter
λ_R	Relaxation time (t)
C	Dimensional constant (t^{-1})
f	Similarity variable
K	Thermal conductivity
M	Magnetic field (Te)
Nu_x	Nusselt number
p	Density of the fluid (kg m^3)
Pr	Prandtl number
Q	Hear source/sink parameter
S	Suctions/injection parameter(ms^{-1})
T	Fluid's temperature (K)
T_∞	Ambient temperature (K)
T_w	Wall temperature (k)
U, V	Velocity components (ms^{-1})
V_1, V_2	Wall velocity
x,y	Cartesian coordinates (I)

***Corresponding Author: Ilyas Khan:** Faculty of Mathematics and Statistics, Ton Duc Thang University, Ho Chi Minh City, Vietnam; Email: ilyaskhan@tdt.edu.vn

Zeeshan Khan, Haroon Ur Rasheed: Sarhad university of Science and Information Technology, Peshawar, KP, 2500, Pakistan

Tawfeeq Abdullah Alkanhal: Department of Mechatronics and System Engineering, College of Engineering, Majmaah University, Majmaah 11952, Saudi Arabia

Murad Ullah: Department of Mathematics, Islamia College University of Pesshawar, KP, 2500, Pakistan

Iskander Tlili: Energy and Thermal Systems Laboratory, National Engineering Scholl of Monastir, Street Ibn El Jazzar, 5019 Monastir, Tunisia

1 Introduction

The flow problem of a hydromagnetic fluid with the effects of porous media and heat transfer is one of the most important problems in the field of engineering and applied sciences. Recently, several mathematicians and applied researchers have proposed that the cooling rate be critical for products in order to improve their quality. For instance, the heat transfer is very important in extracting metal from ores. As a result, a number of field researchers from all of the developed countries recently studied various fluid mechanics problems in different flow configurations, including suction/blowing, magnetohydrodynamics, internal heat generation / absorption, rotation effects, permeability of the porous medium, simultaneous effects of energy and concentration process, viscous dissipations, Joule and Newtonian heating processes, etc. For example, hydromagnetic natural convection flow over a moving surface was studied by Fetecau *et al.* [1]. They presented the radiative heat transfer solution considering the effect of slip boundary conditions. Closed form solutions have been obtained by utilizing the Laplace transform and it was found that the slip parameter has significant effects on the solutions. A note on a Sisko fluid with radiation heat transfer was given by Mehmood and Fetecau [2]. Poiseuille flow was considered in an asymmetric channel and the effect of nonlinear wall temperature was investigated. The expressions for stream functions, axial velocities, and pressure were computed analytically. The micropolar fluid problem was studied by Sheikoleslami *et al.* [3] with heat transfer effects in a channel. The series solution was obtained by the homotopy perturbation method (HPM) and the effects of chemical reactions were investigated. Moreover, the effects of physical quantities such as Reynolds number, Peclet number, and micro rotation was analyzed and discussed through graphs. In another study, the same author [4] used the Differential Transform Method (DTM) for computations considering a micropolar fluid with high mass transfer filled in a porous channel. Ellahi *et al.* [5] analyzed the effects of heat transfer using third grade fluid in a channel. They obtained an analytical solution for axial velocity and temperature distribution for incompressible viscoelastic third grade fluid. Ellahi presented [6] the flow of nanofluid in a circular pipe. The effects of magnetohydrodynamic and variable viscosity are investigated in the solutions. MHD flow of a third grade fluid was investigated by Adesanya and Falade [7]. They explored the heat transfer rate of entropy in two parallel plates. The hydromagnetic slip flow over a shrinking wall of non-Newtonian fluid was computed by Turkyilmazoglu [8]. The dual and triple solutions were obtained. Raza *et al.* [9] presented the rotating flow of nanofluid with the effects of hydromagnetic and slip parameters. Freidoonimehr *et al.* [10] studied unsteady convective flow in a vertical permeable stretching surface with MHD effects. Rashidi *et al.* [11] used a permeable vertical sheet for the MHD free convective flow of non-Newtonian fluid. They presented the effects of radiation and buoyancy in their proposed model. The same author approached the similar procedure to study the mixed convective heat transfer for magnetohydrodynamic viscous fluid with thermal radiation and porous medium [12]. Rashidi *et al.* [13] gave an analytical solution for MHD viscoelastic fluid flow over a stretching surface with continuous motion. For this purpose they applied the homotopy analysis method (HAM). Zahid *et al.* [14] investigated the dual effects of viscous dissipation and thermal radiation on the stagnation point flow induced by an exponentially stretching wall. Awais *et al.* [15] studied the combined effects of Newtonian heating, thermal diffusion and diffusion thermos on an axisymmetric non-Newtonian fluid flow. In the present analysis, we have explored the solution for the internal heat generation/absorption phenomenon of the non-Newtonian Upper-convected-Maxwell fluid flow. The governing equations are first modeled and then solved analytically and numerically. In this context, the constitutive equations for velocity and temperature profiles are solved analytically by applying the homotopy analysis method (HAM).

This technique has already been used for the solution of various problems [16–37]. Ghadikolaei *et al.* [38] studied nonlinear thermal radiation effect on magneto Casson nanofluid flow with joule heating effect over an inclined porous stretching sheet. Hosseinzadeh *et al.* [39] investigated a numerical investigation on ethylene glycol-titanium dioxide nanofluid convective flow over a stretching sheet in presence of heat generation/absorption. Rahmati *et al.* [40] studied dimultaneous investigations the effects of non-Newtonian nanofluid flow in different volume fractions of solid nanoparticles with slip and no-slip boundary conditions. Ghadikolaei *et al.* [41] carried out analytical and numerical solution of non-Newtonian second-grade fluid flow on a stretching sheet. Sheikholeslami *et al.* [42] studied heat transfer improvement and pressure drop during condensation of refrigerant-based nanofluid; an experimental procedure. Guo *et al.* [43] studied numerical study of nanofluids' thermal and hydraulic characteristics considering Brownian motion effect in a micro fin heat sink. Amini *et al.* [44] investigated thermal conductivity of highly porous metal foams using experimental and image based finite element analysis. Tian *et al.* [45] studied heat conduction investigation of functionally graded material

plates with variable gradient parameters under exponential heat source load [46–67].

Furthermore, for the sake of clarity the proposed method is also compared with ND-Solve method [68] and ADM [70, 71]. The effect of modeled parameters such as internal heat generation/absorption, porosity, magnetic parameter, suctions/injection, and Deborah number on the solutions has been shown graphically and discussed. Furthermore, the present result was also compared with published work. A table has been constructed in order to represent the numerical values of a local Nusselt number of different involved physical quantities.

2 Statement of the problem

The system deals with two dimensional steady flow of an Upper-Convected-Maxwell fluid over pa shrinking surface subject to a constant transverse magnetic field B_0. A porous channel is used to show the effects of suction/junction. The fluid saturates the porous medium fo $y > 0$ and the flow occupies the positive region y-axis. The porous medium saturates for > 0 . The shrinking velocity of the wall is $V_1 = -Hw_1$ where and the suction/blowing parameter is represented by V_2. It is pointed out here that $V_2 < 0$ represents suction phenomena while $V_2 > 0$ corresponds to a blowing situation. It is also assumed that the temperature of the wall and free stream conditions are θ_w and θ_∞, respectively. The heat generation or absorption q is also taken into account. In view of these assumptions, the governing basic flow equations are given in the following [1–5]:

$$\frac{\partial u}{\partial x} + \frac{\partial v}{\partial y} = 0, \tag{1}$$

$$u\frac{\partial u}{\partial x} + v\frac{\partial u}{\partial y} + \lambda_R\left(u^2\frac{\partial^2 u}{\partial x^2} + v^2\frac{\partial^2 u}{\partial y^2} + 2uv\frac{\partial^2 u}{\partial x \partial y}\right) = v\frac{\partial^2 u}{\partial y^2} - \frac{\sigma B_0^2}{\rho_f}\left(u + \lambda_R v\frac{\partial u}{\partial y}\right) - \frac{v}{M_p}\left(u + \lambda_R v\frac{\partial u}{\partial y}\right), \tag{2}$$

$$u\frac{\partial T}{\partial x} + v\frac{\partial T}{\partial y} = \alpha\frac{\partial^2 T}{\partial y^2} + \frac{q}{\rho c_p}(T - T_\infty), \tag{3}$$

with the following boundary conditions

$$u = V_1, v = V_2, T = T_w \text{at} y = 0, \tag{4}$$

$$u \to 0, T = T_\infty \text{ at } y \to \infty. \tag{5}$$

u and v are the velocity components along the x and y axes, respectively. Here $V_1 = -cx$ is the shrinking velocity of the wall where $c > 0$ and V_2 is the suction/blowing. Furthermore, (x, y) represents the coordinate system, λ_R is relaxation time, σ is electrical conductivity, B_0 is magnetic field strength, ρ_f is fluid density, M_p is permeability of porous media, T is fluid temperature, α is thermal diffusivity, and c_p is the specific heat. Eqs. (2) and (3) can be transformed into a set of nonlinear ordinary differential equations by introducing the following similarity variables. $u = \frac{\partial \phi}{\partial y}$,

$$u = \frac{\partial \phi}{\partial y},\ v = \frac{\partial \phi}{\partial x},\ \phi = (cv)^{1/2} x f(\eta),\ \eta = \sqrt{\frac{c}{v}}, \tag{6}$$

$$De = \lambda_R c,\ M^2 = \frac{\sigma B_0^2}{c\rho_f},\ S = -V_2/(vc)^{1/2},\ M_p = \frac{v}{cM_p},$$

$$\theta(\eta) = \frac{T - T_\infty}{T_w - T_\infty},\ \alpha = \frac{k}{\rho_f c_p},\ Pr = \frac{v}{\alpha},\ \lambda_H = \frac{q}{c\rho_f c_p}.$$

The transformed ordinary differential equations are

$$f''' - (f')^2 + ff' + De\left(2ff'f'' - f^2 f'''\right) + M^2 Deff'' - M^2 f' - M_p f' + M_p Deff'' = 0, \tag{7}$$

$$\theta'' + \Pr f\theta' + \Pr \lambda_H \theta = 0. \tag{8}$$

The boundary conditions (4) and (5) become

$$f(0) = S, f'(0) = -1, f'(\infty) = 0, \tag{9}$$

$$\theta(0) = 1,\ \theta(\infty) = 0. \tag{10}$$

Here De $= \lambda_R c$ represents the Deborah number in terms of relaxation time, $M^2 = \frac{\sigma {B_0}^2}{c\rho_f}$ is the magnetic parameter, $S = -V_2/(vc)^{1/2}$ is the suction/blowing parameter where $S > 0$ means wall mass suction and $S < 0$ means wall mass injection, $M_p = \frac{v}{cM_p}$ is the porosity parameter, Pr $= \frac{v}{\alpha}$ represents the Prandtl number, $\lambda_H = \frac{q}{c\rho_f c_\rho}$ is the internal heat generation/absorption parameter, and prime represents differentiation with respect to η.

The local Nusselt number Nu_x is the physical quantity of interest for the readers. It is defined as

$$Nu_x = \frac{x q_w}{k(T_w - T_\infty)}, \tag{11}$$

where q_w (the wall heat flux) is defined as

$$q_w = -k\left(\frac{\partial T}{\partial T}\right)_{y=0}. \tag{12}$$

In dimensionless form we can write the above expression as

$$Nu_x/\mathrm{Re}_x^{1/2} = -\theta'(0). \tag{13}$$

3 HAM solution

In order to solve Equations (7) and (8) under the boundary conditions (8) and (10), we utilize the homotopy analysis method (HAM) with the following procedure. The solutions having the auxiliary parameters $\hbar$ regulate and control the convergence of the solutions. The initial guesses are selected as follows:

We select the initial approximation ssuch that the boundary conditionsaare satisfied as follows:

$$f_0(\eta) = s - 1 + e^{-\eta} \text{and} \theta_0(\eta) = e^{-\eta}. \tag{14}$$

The linear operators are introduced as $\Im_f$ and $\Im_\theta$:

$$\Im_f(f) = f' \text{ and } \Im_\theta(\theta) = \theta''. \tag{15}$$

With the following properties:

$$\Im_f(c_1+c_2\eta+c_3\eta^2+c_4e^{-\eta}) = 0 \text{ and } \Im_\theta(c_5+c_6e^{-\eta}) = 0, \tag{16}$$

where $c_i (i = 1 - 6)$ are arbitrary constants in general solution.

The nonlinear operators, according to (7) and (8), are defined as:

$$\begin{aligned}
&\aleph_f\left[f(\eta;p)\right] = \frac{\partial^3 f(\eta;p)}{\partial\eta^3} - \left(\frac{\partial f(\eta;p)}{\partial\eta}\right)^2 \\
&+ f(\eta;p)\frac{\partial f(\eta;p)}{\partial\eta} + De\left(2f(\eta;p)\frac{\partial f(\eta;p)}{\partial\eta}\frac{\partial^2 f(\eta;p)}{\partial\eta^2}\right. \\
&\left.-\left(f(\eta;p)\right)^2\frac{\partial^3 f(\eta;p)}{\partial\eta^3}\right) + \mathrm{M}^2 De\left(f(\eta;p)\frac{\partial^2 f(\eta;p)}{\partial\eta^2}\right) \\
&- \left(\mathrm{M}^2 + \mathrm{M}_p\right)\left(\frac{\partial f(\eta;p)}{\partial\eta}\right) + \mathrm{M}_p De\left(f(\eta;p)\frac{\partial^2 f(\eta;p)}{\partial\eta^2}\right) \\
&= 0, \\
&\aleph_\theta\left[f(\eta;p), \theta(\eta;p)\right] = \frac{\partial^2\theta(\eta;p)}{\partial\eta^2} + \mathrm{Pr} f\frac{\partial\theta(\eta;p)}{\partial\eta} \\
&+ \mathrm{Pr}\lambda_H\theta(\eta;p).
\end{aligned} \tag{17}$$

The auxiliary function becomes

$$\mathrm{H}_f(\eta) = \mathrm{H}_\theta(\eta) = e^{-\eta}. \tag{18}$$

The symbolic software Mathematica is employed to solve ith order deformation equations:

$$\begin{aligned}
\Im_f\left[f_i(\eta) - \chi_i f_{i-1}(\eta)\right] &= \hbar_f\mathcal{H}_f\left[f(\eta)\right]R_{f,i}(\eta), \\
\Im_\theta\left[\theta_i(\eta) - \chi_i\theta_{i-1}(\eta)\right] &= \hbar_\theta\mathcal{H}_\theta(\eta)R_{\theta,i},
\end{aligned} \tag{19}$$

where $\hbar$ is auxiliary non-zero parameter and

$$\begin{aligned}
R_{f,i}(\eta) &= f'''_{m-1} - \sum_{k=0}^{m-1} f'_{m-1-k}f'_k + \sum_{k=0}^{m-1} f_{m-1-k}f'_k \\
&+ 2De\left(\sum_{k=0}^{m-1} f_{m-1-k}\sum_{l=0}^{k} f'_{k-l}f''_l - \sum_{k=0}^{m-1} f_{m-1-k}\sum_{l=0}^{k} f'_{k-l}f'''_l\right) \\
&+ De\left(M^2 + M_p\right)\sum_{k=0}^{m-1} f'_{m-1-k}f''_k - \left(M^2 + M_p\right)f', R_{\theta,i}(\eta) \\
&= \theta''_{m-1} + \mathrm{Pr}\sum_{k=0}^{m-1} f_{m-1-k}\theta'_k + \mathrm{Pr}\lambda_H\theta_{m-1},
\end{aligned} \tag{20}$$

$$\chi_i = \begin{cases} 0, \text{if } i \le 1 \\ 1, \text{if } i > 1, \end{cases}$$

are the involved parameters in HAM theory (for more information about the different steps of HAM see [16–24]).

To control and speed the convergence of the approximation series by the help of the so-called h-curve, it is significant to choose a proper value of auxiliary parameter. The calculation are carried out on a personal computer with 4GB RAM and 2.70GHz CPu. The h-curves of $f(0)$ and $\theta\prime(0)$ obtained by the 18th order of HAM solution are shown in Figure 1 which take approximately less than a minute in the exicution. To obtain the optimal values of auxiliary parameters, the averaged residual errors are defined as

$$\begin{aligned}
\mathrm{Re}_f &= \frac{d^3 f(\eta)}{\delta\eta^3} - \left(\frac{df(\eta)}{\delta\eta}\right)^2 + f(\eta)\frac{df(\eta)}{\delta\eta} \\
&+ De\left(2f(\eta)\frac{df(\eta)}{d\eta}\frac{d^2 f(\eta)}{\partial\eta^2} - \left(f(\eta)\right)^2\frac{d^3 f(\eta)}{d\eta^3}\right) \\
&+ \mathrm{M}^2 De\left(f(\eta)\frac{d^2 f(\eta)}{d\eta^2}\right) - \left(\mathrm{M}^2 + \mathrm{M}_p\right)\left(\frac{\partial f(\eta)}{d\eta}\right) \\
&+ \mathrm{M}_p De\left(f(\eta)\frac{d^2 f(\eta)}{d\eta^2}\right) = 0,
\end{aligned} \tag{21}$$

$$\mathrm{Re}_\theta = \frac{d^2\theta(\eta)}{d\eta^2} + \mathrm{Pr} f\frac{d\theta(\eta)}{d\eta} + \mathrm{Pr}\lambda_H\theta(\eta). \tag{22}$$

In order to survey the accuracy of the present method, the residual errors for the 20th order of HAM solutions of (21) and (22) are illustrated in Figures 2 and 3, and listed numerically in Table 1. An efficient numerical (ND-Solve) method is also applied to solve the transformed equations (7) and (8) correspond ding to the boundary conditions given in equations (9) and (10) and compared with a HAM solution graphically and numerically as shown in Figures 4-5 and Tables 1-2, respectively.

4 Results and discussion

The transformed equations (7) and (8) subject to the boundary conditions (9) and (10) are solved analytically

Table 1: Numerical comparison of HAM and numerical method for $f(\eta)$ when $s = 1.5$

η	HAM	Numerical Solution	Absolute error
0	1.5	1.5	0
1	0.363339	0.295145	0.2*E−5
2	0.142604	0.054937	0.7*E−5
3	0.064857	0.014492	0.5*E−5
4	0.036777	0.033891	0.8*E−5
5	0.026519	0.037965	0.4*E-7
6	0.022756	0.033713	0.3*E−6
7	0.021372	0.01227	0.5*E−8

Table 2: Numerical comparison of HAM and numerical method for $\theta(\eta)$ when $s = 1$, $De = M_p = 0.1$, $\lambda_H = 0.2$, $M = 0.2$, $R = 0.3$ and $\Pr = 0.5$

η	HAM	Numerical Solution	Absolute error
0	1	1	0
1	0.394107	0.383863	0.4*E−6
2	0.147016	0.0968637	0.1*E−6
3	0.054222	0.018324	0.1*E−7
4	0.0199581	0.00242894	0.3*E−9
5	0.00734324	5.14998*E−9	0.2*E−11
6	0.00270155	−0.000160322	0.3*E−8
7	0.000993861	−0.0000814985	0.1*E−10

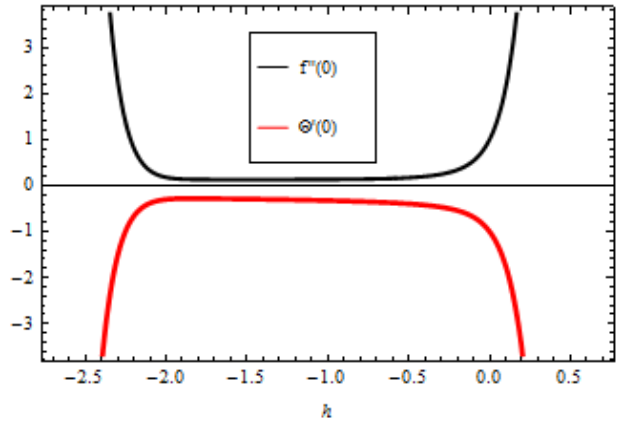

Figure 1: The $\hbar$-curve of $f(0)$ and $\theta\prime(0)$ obtained by the 18th order of HAM solution when $De = M_p = \lambda_H = 0.1$, $M = 0.2$, $R = 0.3$ and $\Pr = 0.5$

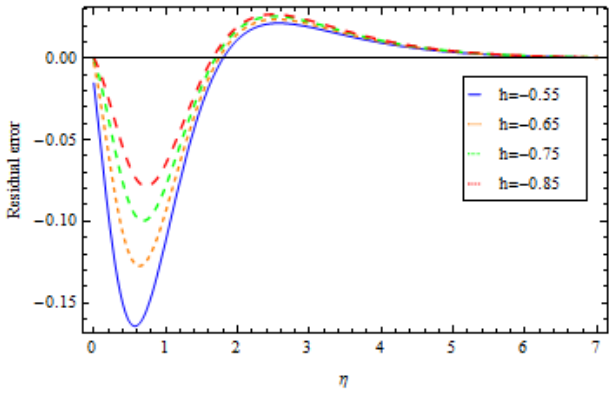

Figure 2: Residual error of Eq. (21) when $De = M_p = \lambda_H = 0.1$, $M = 0.2$, $R = 0.3$ and $\Pr = 0.5$

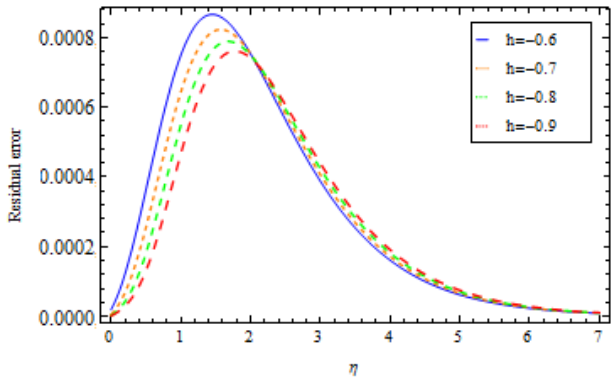

Figure 3: Residual error of Eq. (22) when $De = M_p = \lambda_H = 0.1$, $M = 0.2$, $R = 0.3$ and $\Pr = 0.5$

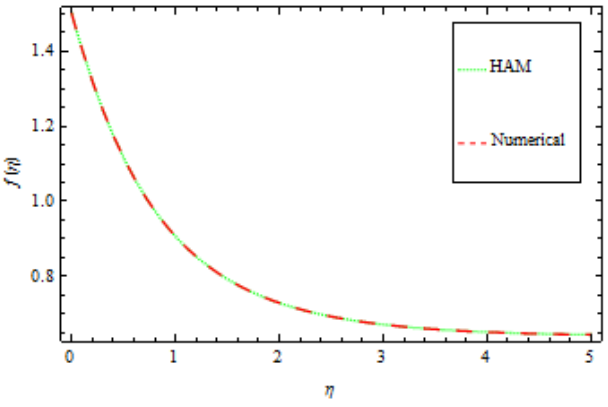

Figure 4: Comparison between HAM and Numerical solutions for velocity profile $f(\eta)$ when $s = 1.5$, $De = M_p = 0.1$, $\lambda_H = 0.2$, $M = 0.2$ and $R = 0.3$

by the homotopy analysis method. An efficient numerical method called ND-Solve method is also used for the sake of comparison. In this section, numerical values are assigned to the physical parameters involved in the velocity, temperature and local Nusselt number. The paper examined the effects of governing parameters on the transient velocity profile, temperature profile and local Nusselt number. For this purpose the SRM approach has been applied for

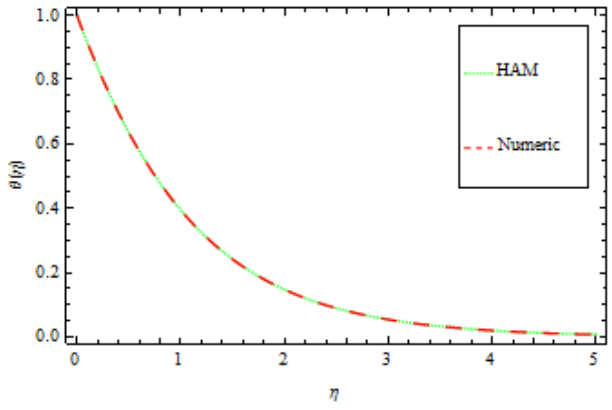

Figure 5: Comparison between HAM and Numerical solutions for temperature profile $\theta(\eta)$ when $s = 1$, $De = M_p = 0.1$, $\lambda_H = 0.2$, $M = 0.2$, $R = 0.3$ and $\Pr = 0.5$

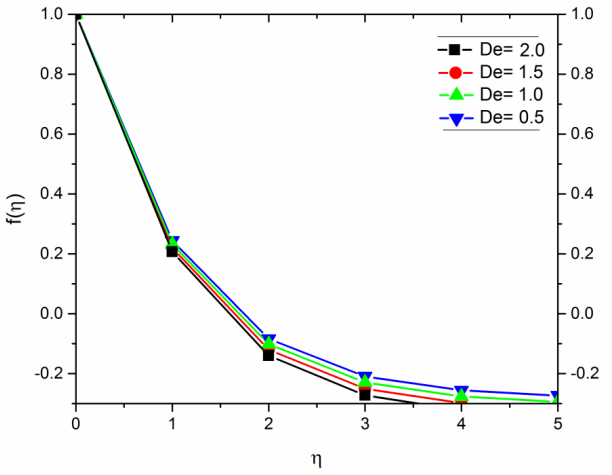

Figure 6: Effect of De on velocity profile f when $S = 1$, $M_p = 0.3$, $M = 0.1$

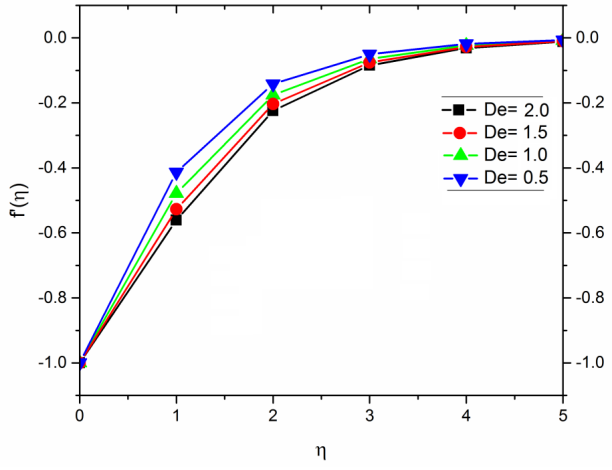

Figure 7: Effect of De on velocity profile f' when $S = 1$, $M_p = 0.3$, $M = 0.1$

various values of flow controlling parameters $De = 0.1$, $M_p = 0.3$, $\lambda_H = 0.2$, $M = 0.2$, $R = 0.3$ and $\Pr = 0.5$, to obtain a clear insight into the physics of the problem. Therefore, all the graphs and tables correspond to the values above and the rest will be mentioned.

Figures 6 and 7 show the influence of Deborah number De on the velocities f and f' respectively. It is obvious from these figures that the boundary layer thickness decreases for larger values of De, with an increase in η. Physically, viscous effects increase for the larger Deborah numbers. These retard the flow in the entire domain and consequently the momentum boundary layer will be thinner. Since the Deborah number defines the difference between the solids and liquid (or fluids), the material shows fluid like behavior for a small Deborah number and for larger values of Deborah number the material behaves like a viscoelastic solid such as rubber, jelly, polymers etc. From the present analysis it is quite obvious that the velocity field decelerating for larger numbers.

Figure 8 and 9 depict the effects of porosity parameter M_p on f and f' respectively. It is observed that the velocity profile increases with increasing porosity parameter. Small variation is observed for f'. Furthermore, under the influence of constant magnetic field $M = 0.3$, the momentum boundary layer decreases due to the Lorentz force.

Figures 10 and 11 present the effects of suction/injection parameter s on f and f'. It is noticed that the velocity fields f and f' satisfy the far field boundary conditions (9) asymptotically, thus verifying the analytical and numerical results obtained.

Figure 12 displays the influence of magnetic field on the velocity profiles f with $s = 1$, $De = 0.1$, $M_p = 0.3$, $M = 0.2$ and $R = 0.3$. Due to the inflection of the vertical magnetic field to the electrically conducting fluid, the Lorentz force is produced. This force has the tendency to slow down the flow and as a result the velocity profile decreases. Figures 13-**??** show the effect of different parameters on the temperature profiles. The effect of Prandtl number on the temperature distribution is shown in Figure 13. Based on the Prandtl number's definition $\Pr = \frac{\nu}{\alpha}$, this parameter is defined as the ratio between the momentum diffusion to thermal diffusion. Thus, with the increase of Prandtl number the thermal diffusion decreases and so the thermal boundary layer becomes thinner as seen in Figure 13. It physically means that the flow with a large Prandtl number dissipates the heat faster to the fluid as the temperature gradient gets steeper and hence increases the heat transfer coefficient between the surface and the fluid. Figure 14 depicts the variation of Deborah number on the

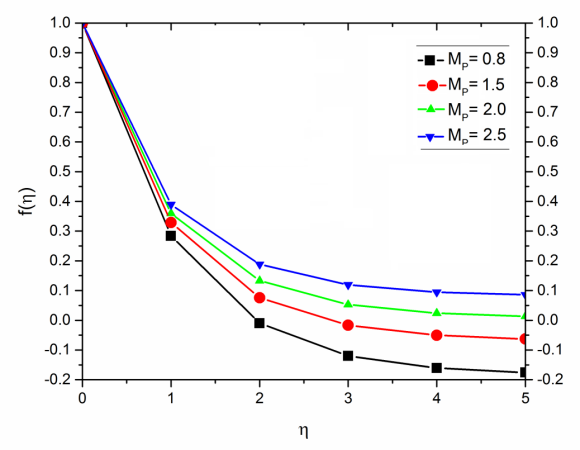

Figure 8: Effect of M_p on velocity profile f when $S = 1$, $De = 0.5$, $M = 0.1$

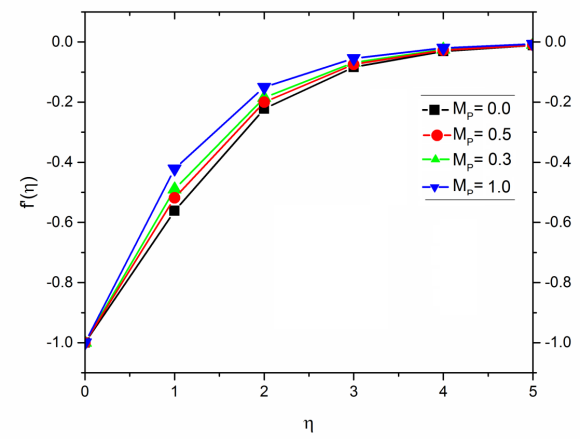

Figure 9: Effect of M_p on velocity profile f' when $S = 1$, $De = 0.5$, $M = 0.1$

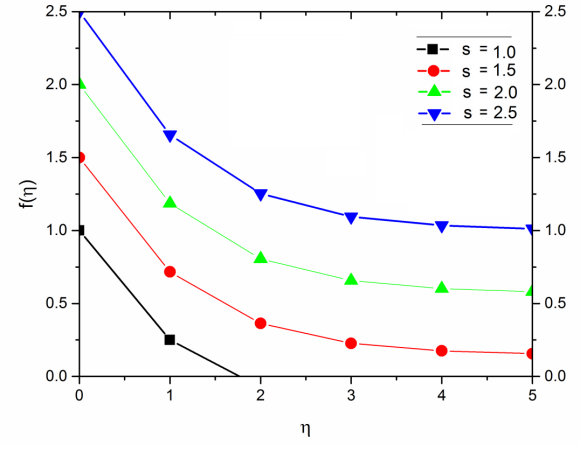

Figure 10: Effect of S on velocity profile f when $M_p = 0.2$, $De = 0.5$, $M = 0.1$

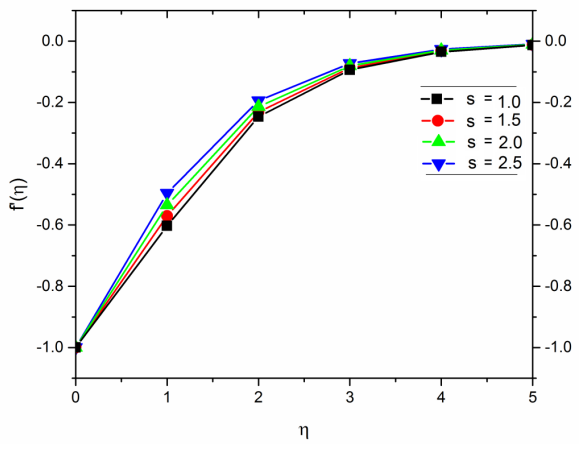

Figure 11: Effect of S on velocity profile f' when $M_p = 0.2$, $De = 0.5$, $M = 0.1$

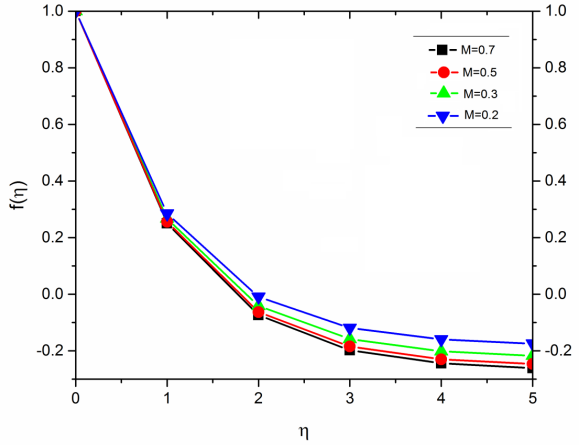

Figure 12: Effect of M on velocity profile f when $M_p = 0.2$, $De = 0.5$, $S = 1$

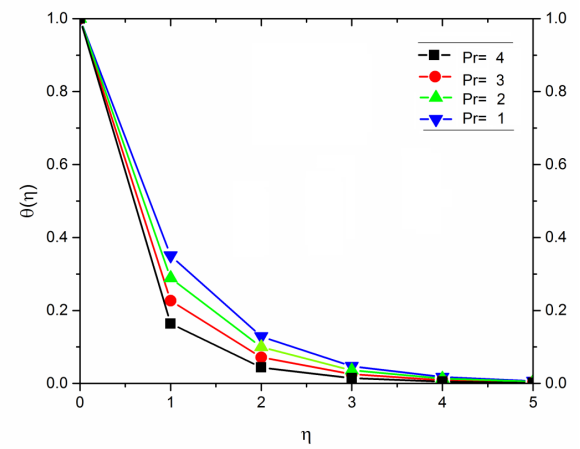

Figure 13: Effect of Pr on temperature profile θ when $M_p = 0.2$, $De = 0.5$, $S = 2$, $M = 0.3$, $\lambda_H = 0.2$

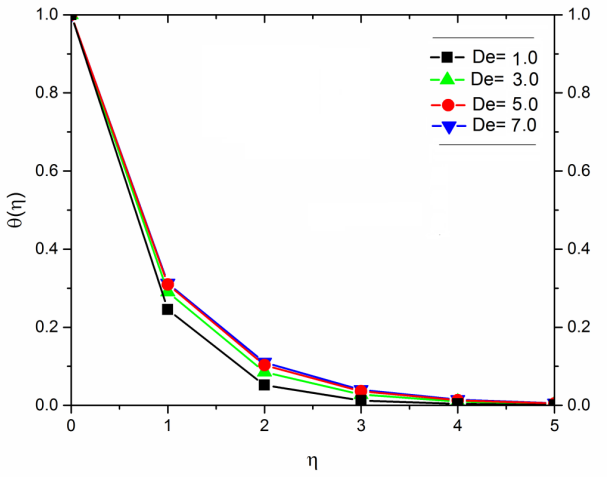

Figure 14: Effect of De on temperature profile θ when $M_p = 0.2$, $S = 2$, Pr $= 0.5$, $M = 0.3$, $\lambda_H = 0.2$

temperature distribution. Increasing the Deborah number De increases the temperature inside the fluid. Also, it is observed that for larger values of Deborah number the boundary layer thickness decreases with increasing η.

The influence of magnetic parameter M on the temperature distribution is shown in Figure 15. It is observed that the temperature distribution increases with increasing values of magnetic parameter M. Physically, the Lorentz force due to the transverse magnetic field has the property of relaxing the fluid velocity and temperature distributions. Accordingly, the velocity and temperature boundary layer thickness decreases as the magnetic parameter increases.

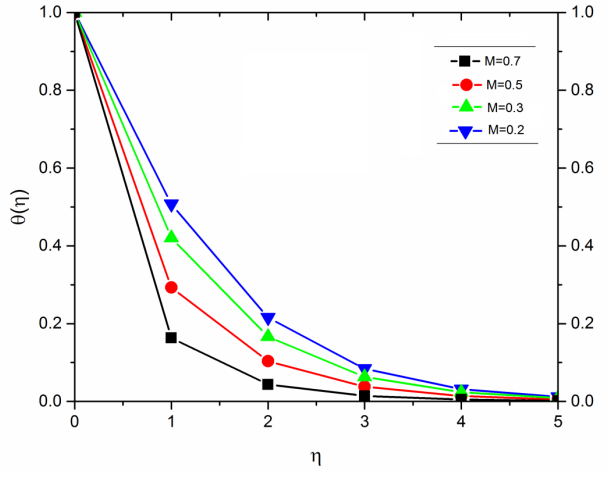

Figure 15: Effect of M on temperature profile θ when $M_p = 0.2$, $S = 2$, Pr $= 0.5$, $De = 0.2$, $\lambda_H = 0.2$

The effect of the porous permeability parameter M_p on the fluid temperature distribution is shown in Figure 16. The result shows that as the porous permeability parameter increases, there is a corresponding increase in the fluid temperature due to increased diffusion of heat within the flow channel.

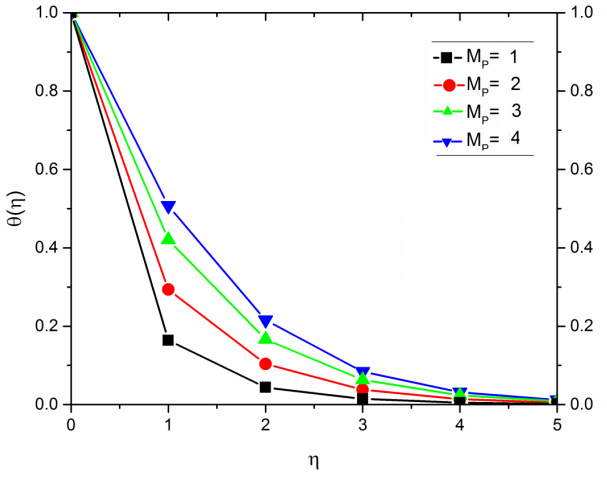

Figure 16: Effect of M_p on temperature profile θ when $M = 0.1$, $S = 2$, Pr $= 0.5$, $De = 0.2$, $\lambda_H = 0.2$

The effect of heat source ($\lambda_H > 0$) and heat sink ($\lambda_H < 0$) parameters are shown in Figures 17 and 18 respectively. It is observed that a heat source enhances the thermal conductivity and increases the fluid temperature as shown in Figure 13. Figure 14 incorporates the effects of the heat sink parameter. As expected, a heat sink provides a decrease in the fluid temperature.

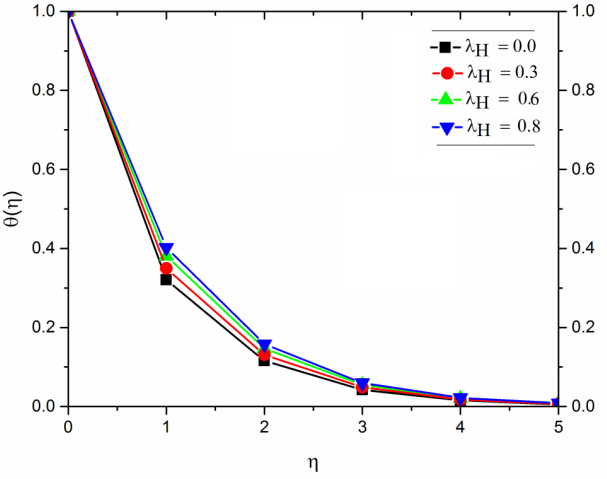

Figure 17: Effect of heat generation $\lambda_H > 0$ on temperature profile θ when $M = 0.1$, $S = 2$, Pr $= 0.5$, $De = 0.2$

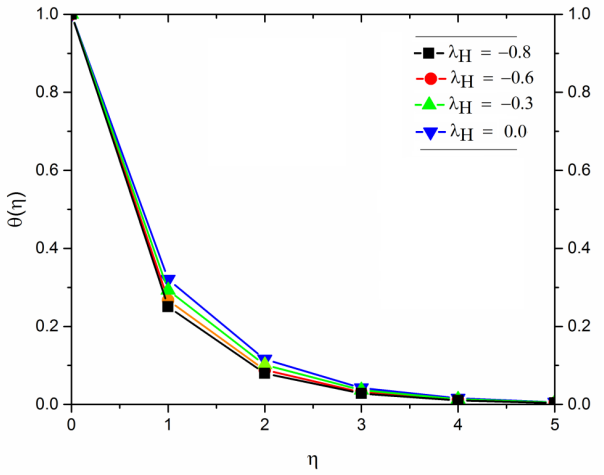

Figure 18: Effect of heat absorption $\lambda_H < 0$ on temperature profile θ when $M = 0.1$, $S = 2$, $\Pr = 0.5$, $De = 0.2$

Table 3 shows different values of skin friction parameter $-f^{(0)}$ for several values of permeability parameter M_p. We see from this table that the magnitude of shear stress in the boundary is smaller for injection in comparison to the case of suction. These results are in accordance with the physical situation because the injection of the fluid amounts to an increase of fluid velocity, resulting in a decrease of the frictional force. The permeability parameter introduces additional shear stress on the boundary. Note that the increase of permeability parameter leads to the increase of skin friction parameter in all the cases of suction, blowing, and impermeability of the surface.

Table 3: Values of skin friction parameter $-f^{(0)}$ for several values of permeability parameter M_p when $De = 0.1$, $M = 0.2$

s	M_p	$-f^{(0)}$
1.2	0	3
	1	3.56785
	2	4.825621
0	0	2
	1	2.05710
	2	2.402051
−1.5	0	1.7
1	1.801261	
2	1.913583	

In order to discuss the results of local Nusselt number against different physical quantities including Deborah number, Prandtl number, and internal heat generation/absorption quantity, we have prepared Table 4. It is evident from this table that the local Nusselt number decreases due to an increase in Deborah number and quantity oif internal heat generation/absorption, whereas the local Nusselt number increases due to an increase in Prandtl number.

Table 4: Effect of various physical quantities on local Nusselt number $-\theta'(0)$ including Deborah number, Prandtl number Pr and internal heat generation/absorption parameter λ_H

De	Pr	λ_H	$-\theta'(0)$
0.0	1.0	0.2	2
0.1			1.283923
0.2			1.329046
0.1	0.1		0.163950
	0.5		1.320615
	1.2		2.325102
	0.1	−0.3	2.031823
		−0.1	1.325165
		0.2	2.290552
		0.4	1.221048

5 Conclusion

In this research paper, the semi-analytical/numerical technique known as HAM has been implemented to solve the transformed nonlinear differential equations describing the MHD flow of an Upper-Convected-Maxwell fluid with the influence of the internal heat generation/absorption. The dynamics of the magneto-hydrodynamic fluid flow in porous medium over a porous wall are investigated. The present semi-numerical/analytical simulations agree closely with the previous studies for some special cases. HAM has been shown to be a very strong and efficient technique in finding analytical solutions for nonlinear differential equations. HAM is shown to illustrate excellent convergence and accuracy and is currently being employed to extend the present study to mixed convective heat transfer simulations. The convergence of the series solution is established. Furthermore, the present method is also compared with an efficient numerical technique so called ND-Solve method. The effects of different physical key parameters which effect fluid motion such as Deborah number, magnetic parameter, suction/injection parameter, heat generation/absorption parameter, and porosity parameter are plotted and discussed. It is observed that with the increasing Deborah number the velocity decreases and the temperature inside the fluid increases. The

results show that the velocity and temperature distribution increases with a porous medium. It is also investigated that the magnetic parameter has a decelerating effect on velocity while the temperature profiles increases in the entire domain. Due to increase in Prandtle number the temperature profile increases. It is observed that the heat source enhance the thermal conductivity and increases the fluid temperature while the heat sink provides a decrease in the temperature fluids.

References

[1] Fetecau C., Vieru D., Fetecau C. and Akhter S. General solutions for the magneto-hydrodynamic natural convection flow with radiative heat transfer and slip conditions over a moving plate, Z. Natur-forsch., 2013, 68a, 659-667.

[2] Mehmood O., Fetecau C. A note on radiative heat transfer to peristaltic flow of Sisko fluid, Appl. Bionics Biomech., 2015, 283892.

[3] Sheikholeslami M., Hatami M., Ganji D.D., Micropolar fluid flow and heat transfer in a permeable channel using analytical method, J. Mol. Liquids., 2014, 194, 30-36.

[4] Sheikholeslami M., Ashorynejad H.R., Ganji D.D., Rashidi M.M., Heat and mass transfer of amicropolar fluid in a porous channel, Comm. Numer. Anal., 2014, 00166.

[5] Ellahi R., Ariel P.D., Hayat T., Asghar S., Effects of heat transfer on a third-grade fluid in a flat channel, Int. J. Numer. Meth. Fluids., 2010, 63, 847-850.

[6] Ellahi R., The effects of MHD and temperature dependent viscosity on the flow of non-Newtonian nanofluid in a pipe: Analytical solutions, App. Math. Mod., 2013, 37, 1451-1467.

[7] Ad esanya S. O., Falade J. A., Thermodynamics analysis of hydromagnetic third grade fluidflow through channel filled with porous medium. Alex. Eng. J., 2015, 54, 615-622.

[8] Turkyilmazoglu M., Dual and triple solutions for MHD slip flow of non-Newtonian fluid over a shrinking surface, Comp. Fluids., 2012, 70, 53-58.

[9] Raza J, Rohni A. M., Omar Z., Awais M., Heat and mass transfer analysis of MHD Nanofluid flow in a rotating channel with slip effects, J. Mol. Liq., 2016, 219, 703-708.

[10] Freidoonimehr N., Rashidi M. M., Mahmud S., Unsteady MHD free convective flow past a permeable stretching vertical surface in a nano-fluid, Int. J. Therm. Sci., 2015, 87, 136-145.

[11] Rashidi M.M., Rostami B., Freidoonimehr N., Abbasbandy S., Free convection heat and mass transfer for MHD fluid flow over a permeable veritical stretching sheet in the presence of radiation andbuoyancy effects, Ain Shams Eng. J., 2014, 6, 901-912.

[12] Rashidi M.M., Ali M., Freidoonimehr N., Rostami B., Hossain M.A., Mixed convective heat trans-fer for MHD viscoelastic fluid flow over a porous wedge with thermal radiation, Adv. Mech. Eng., 2014, 735939.

[13] Rashidi M. M., Momoniat E., Rostami B., Analytic approximate solutions for MHD boundary-layer viscoelastic fluid flow over continuously moving stretching surface by homotopy analysis method with two auxiliary parameters, J. Appl. Math., 2012, 780415.

[14] Iqbal Z., Qasim M., Awais M., Hayat T., Asghar S., Stagnation-point flow by an exponentially stretching sheet in the presence of viscous dissipation and thermal radiation, J. Aerospace Eng., 2015, 29(2).

[15] Awais M., Hayat T., Nawaz M., Alsaedi A., Newtonian heating, thermal-diffusion and diffusion-thermo effects in an axisymmetric flow of a Jeffery fluid over a stretching surface, Braz. J. Chem. Eng., 2015, 32, 555-561.

[16] Ahmadi M. H., Ahmadi M. A., Pourfayaz F., Hosseinzade H., Acıkkalp E., Tlili I., Michel F., Designing a powered combined Otto and Stirling cycle power plant through multi-objective optimization approach, Renew. Sustain. Ener. Rev., 2016, 62, 585-595.

[17] Tlili I., Timoumi Y., Ben Nasrallah S., Numerical simulation and losses analysis in a Stirling engine, Int. J. Heat Technol., 2006, 24, 1.

[18] Tlili I., Timoumi Y, Ben Nasrallah S., Thermodynamic analysis of Stirling heat engine with regenerative losses and internal irreversibilities, Int. J. Engine Res., 2007, 9, 45-56.

[19] Timoumi Y., Tlili I., Ben Nasrallah S., Performance optimization of Stirling engines Renew. Ener., 2008, 2134-2144.

[20] Tlili I., Renewable energy in Saudi Arabia: current status and future potentials, Environment, development and sustainability, 2015, 17(4), 859-886.

[21] Sa'ed A., Tlili I., Numerical Investigation of Working Fluid Effect on Stirling Engine Performance, Int. J. Therm. Envir. Eng., 2015, 10(1), 31-36.

[22] Tlili I., Finite time thermodynamic evaluation of endoreversible Stirling heat engine at maximum power conditions, Renew. Sustain. Ener. Rev., 2012, 16(4), 2234-2241.

[23] Tlili I., Thermodynamic Study on Optimal Solar Stirling Engine Cycle Taking Into Account The Irreversibilities Effects, Ener. Proc., 2012, 14, 584-591.

[24] Tlili I., A numerical investigation of an alpha Stirling engine, Int. J. Heat Technol., 2012, 30(1), 23-35.

[25] Tlili I., Musmar S.A., Thermodynamic evaluation of a second order simulation for Yoke Ross Stirling engine, Ener. Conv. Manag., 2013, 68, 149-160.

[26] Tlili I., Timoumi Y., Nasrallah S.B., Analysis and design consideration of mean temperature differential Stirling engine for solar application, Renew. Ener., 2008, 33, 1911-1921.

[27] Timoumi Y., Tlili I., Nasrallah S.B., Design and performance optimization of GPU-3 Stirling engines, Energy, 2008, 33, 1100-1114.

[28] Timoumi Y., Tlili I., Nasrallah S. B., Reduction of energy losses in a Stirling engine, Heat Technol., 2007, 25, 1, 84-93.

[29] Al-Qawasmi A. R., Tlili I., Energy Efficiency Audit Based on Wireless Sensor and Actor Networks: Air-Conditioning Investigation, J. Eng., 2018, 2, 3640821.

[30] Al-Qawasmi A.R., Tlili I., Energy efficiency and economic impact investigations for air-conditioners using wireless sensing and actuator networks, Ener. Rep., 2018, 4, 478-485.

[31] Khan M.N., Khan W., Tlili I., Forced Convection of Nanofluid Flow Across Horizontal Elliptical Cylinder with Constant Heat Flux Boundary Condition, J. Nanofluids, 2019, 8(2), 1-8.

[32] Tlili I., Khan W., Ramadan K., MHD Flow of Nanofluid Flow Across Horizontal Circular Cylinder: Steady Forced Convection, J. Nanofluids, 2019, 8(1), 179-186.

[33] Afridi M.I., Tlili I., Qasim M., Khan I., Nonlinear Rosseland thermal radiation and energy dissipation effects on entropy generation in CNTs suspended nanofluids flow over a thin needle,

Bound. Value Probl. 2018, 148.
[34] Almutairi M.M., Osman M., Tlili I., Thermal Behavior of Auxetic Honeycomb Structure: An Experimental and Modeling Investigation, ASME. J. Ener. Res. Technol., 2018, 140(12), 122904-122908.
[35] Zhixiong L., Khan I., Shafee A., Tlili I., Asifa T., Energy transfer of Jeffery-Hamel nanofluid flow between non-parallel walls using Maxwell-Garnetts (MG) and Brinkman models, Ener. Rep., 2018, 4, 393-399.
[36] M.N. Khan, Tlili I., Innovative thermodynamic parametric investigation of gas and steam bottoming cycles with heat exchanger and heat recovery steam generator: Energy and exergy analysis, Ener. Rep., 2018, 4, 497-506.
[37] Ali F., Aamina, Khan I., Sheikh N.A., Gohar M., Tlili I., Effects of Different Shaped Nanoparticles on the Performance of Engine-Oil and Kerosene-Oil: A generalized Brinkman-Type Fluid model with Non-Singular Kernel, Sci. Rep., 2018, 8, 15285.
[38] Ghadikolaei S.S., Hosseinzadeh K., Ganji D.D., Jafari B., Nonlinear thermal radiation effect on magne to Casson nanofluid flow with Joule heating effect over an inclined porous stretching sheet, Case Studies Therm. Eng., 2018, 12, 176-187.
[39] Hosseinzadeh K., Afsharpanah F., Zamani S., Gholinia M., Ganji D.D., A numerical investigation on ethylene glycol-titanium dioxide nanofluid convective flow over a stretching sheet in presence of heat generation/absorption, Case Studies Therm. Eng., 2018, 12, 228-236.
[40] Rahmati A.R., Akbari O.A., Marzban A., Toghraie D., Karimi R., Pourfattah F., Simultaneous investigations the effects of non-Newtonian nanofluid flow in different volume fractions of solid nanoparticles with slip and no-slip boundary conditions, Therm. Sci. Eng. Prog., 2018, 5, 263-277.
[41] Ghadikolaei S.S., Hosseinzadeh K., Yassaria M., Sadeghia H., Ganjib D.D., Analytical and numerical solution of non-Newtonian second-grade fluid flow on a stretching sheet, Therm. Sci. Eng. Prog., 2018, 5, 308-316.
[42] Sheikholeslami M., Darzi M., Sadoughi M.K., Heat transfer improvement and pressure drop during condensation of refrigerant-based nanofluid; an experimental procedure, Int. J. Heat Mass Transf., 2018, 122, 643-650.
[43] Guo W., Li G., Zheng Y., Dong C., Numerical study of nanofluids thermal and hydraulic characteristics considering Brownian motion effect in micro fin heat sink, J. Mol. Liq., 2018, 254, 446-462.
[44] Amini Y., Takahashi A., Chantrenne P., Maruyama S., Dancette S., Maire E., Thermal conductivity of highly porous metal foams: Experimental and image based finite element analysis., Int. J. Heat Mass Transf., 2018,122, 1-10.
[45] Tian J.H., Jiang K., Heat conduction investigation of the functionally graded materials plates with variable gradient parameters under exponential heat source load, Int. J. Heat Mass Transf., 2018, 122, 22-30.
[46] Tlili I., Khan W., Ramadan K., Entropy Generation Due to MHD Stagnation Point Flow of a Nanofluid on a Stretching Surface in the Presence of Radiation, J. Nanofluids, 2018, 7(5), 879-890.
[47] Asif M., Haq S., Islam S., Khan S., Tlili I., Exact solution of non-Newtonian fluid motion between side walls, Res. Phys., 2018, 11, 534-539.
[48] Agaie B.G., Khan I., Yacoob Z., Tlili I., A novel technique of reduce order modelling without static correction for transient flow of non-isothermal hydrogen-natural gas mixture, Res. Phys., 2018, 10, 532-540.
[49] Khalid A, Khan I., Khan A., Shafie S., Tlili I., Case study of MHD blood flow in a porous medium with CNTS and thermal analysis, Case Studies Therm. Eng., 2018, 12, 374-380.
[50] Khan I., Abro K.A., Mirbhar M.N., Tlili I., Thermal analysis in Stokes' second problem of nanofluid: Applications in thermal engineering, Case Studies Therm. Eng., 2018, 12, 271-275.
[51] Afridi M.I., Qasim M., Khan I., Tlili I., Entropy generation in MHD mixed convection stagnation-point flow in the presence of joule and frictional heating, Case Studies Therm. Eng., 2018, 12, 292-300.
[52] Khan M.N., Tlili I., New advancement of high performance for a combined cycle power plant: Thermodynamic analysis, Case Studies in Thermal Engineering, 2018, 12, 166-175.
[53] Khan M.N., Tlili I., Performance enhancement of a combined cycle using heat exchanger bypass control: A thermodynamic investigation, J. Clean. Prod., 2018, 192(10), 443-452.
[54] Khan Z.A., Haq S., Khan T.S., Khan I., Tlili I., Unsteady MHD flow of a Brinkman type fluid between two side walls perpendicular to an infinite plate, Res. Phys., 2018, 9, 1602-1608.
[55] Aman S., Khan I., Ismail Z., Salleh M.Z., Tlili I., A new Caputo time fractional model for heat transfer enhancement of water based graphene nanofluid: An application to solar energy, Res. Phys., 2018, 9, 1352-1362.
[56] Khan Z., Khan I., Ullah M., Tlili I., Effect of thermal radiation and chemical reaction on non-Newtonian fluid through a vertically stretching porous plate with uniform suction, Res. Phys., 2018, 9, 1086-1095.
[57] Khan I., Tlili I., Imran M.A., Miraj F., MHD fractional Jeffrey's fluid flow in the presence of thermo diffusion, thermal radiation effects with first order chemical reaction and uniform heat flux, Res. Phys. 2018, 10, 10-17.
[58] Tlili I., Khan W., Khan I., Multiple slips effects on MHD SA-Al2O3 and SA-Cu non-Newtonian nanofluids flow over a stretching cylinder in porous medium with radiation and chemical reaction, Res. Phys., 2018, 8, 213-222.
[59] Khan Z., Rasheed H., Tlili I., Khan I., Abbas T., Runge-Kutta 4th-order method analysis for viscoelastic Oldroyd 8-constant fluid used as coating material for wire with temperature dependent viscosity, Sci. Rep., 2018, 8(8), 14504.
[60] Tlili I., Hamadneh N.N., Khan W.A., Thermodynamic Analysis of MHD Heat and Mass Transfer of Nanofluids Past a Static Wedge with Navier Slip and Convective Boundary Conditions, Arab. J. Sci. Eng., 2018, 1-13.
[61] Tlili I., Hamadneh N.N., Khan W.A., Atawneh S., Thermodynamic analysis of MHD Couette-Poiseuille flow of water-based nanofluids in a rotating channel with radiation and Hall effects, J. Therm. Anal. Calorim., 2018, 132(3), 1899-1912.
[62] Khan M.N., Tlili I., Khan W., Thermodynamic Optimization of New Combined Gas/Steam Power Cycles with HRSG and Heat Exchanger, Arabian J. Sci. Eng., 2017, 42(11), 4547-4558.
[63] Makinde O.D., Tlili I., Mabood F., Khan W., Tshehla M.S., MHD Couette-Poiseuille flow of variable viscosity nanofluids in a rotating permeable channel with Hall effects, J. Mol. Liq., 2016, 221, 778-787.
[64] Sa'ed A., Musmar A.T., Al-Halhouli, Tlili I., Büttgenbach S., Performance Analysis of a New Water-based Microcooling System, Exp. Heat Transf., 2016, 29(4), 485-499.
[65] Ramadan K., Tlili I., Shear work, viscous dissipation and axial conduction effects on microchannel heat transfer with a con-

stant wall temperature, Proc. Instit. Mech. Eng., Part C: J. Mech. Eng. Sci., 2016, 230(14), 2496-2507.

[66] Ramadan K., Tlili I., A Numerical Study of the Extended Graetz Problem in a Microchannel with Constant Wall Heat Flux: Shear Work Effects on Heat Transfer, J. Mech., 31(6), 733-743.

[67] Musmar S.A., Razavinia N., Mucciardi F., Tlili I., Performance analysis of a new Waste Heat Recovery System, Int. J. Therm. Envir. Eng., 2015, 10, 31-6.

[68] Khan W., Gul T., Idrees M., Islam S., Khan I., Dennis L.C.C. Thin Film Williamson Nanofluid Flow with Varying Viscosity and Thermal Conductivity on a Time-Dependent Stretching Sheet, Appl. Sci., 2016.

[69] Adomian G., Review of the Decomposition Method and Some Recent Results for Non-Linear Equations, Math. Comput. Model., 1992, 13 287-299.

[70] Wazwaz A.M., Adomian Decomposition Method for a Reliable Treatment of the Bratu-Type Equations, Appl. Math. Comput., 2005, 166 652-663.

[71] Wazwaz A.M., Adomian Decomposition Method for a Reliable Treatment of the Emden-Fowler Equation, Appl. Math. Comput., 2005, 161 543-560.